Bull. Mater. Sci., Vol. 34, No. 3, June 2011, pp. 507–513. © Indian Academy of Sciences.

Post irradiated microstructural characterization of Zr–1Nb alloy by X-ray diffraction technique and positron annihilation spectroscopy

P S CHOWDHURY, P MUKHERJEE*, N GAYATHRI, M BHATTACHARYA, A CHATTERJEE, P BARAT and P M G NAMBISSAN†

Variable Energy Cyclotron Centre, 1/AF Bidhan Nagar, Kolkata 700 064, India
†Saha Institute of Nuclear Physics, 1/AF Bidhan Nagar, Kolkata 700 064, India

MS received 12 September 2010; revised 22 December 2010

Abstract. **Zr–1Nb samples were irradiated with 116 MeV O^{5+} ions at different doses ranging from 5×10^{17} to 8×10^{18} O^{5+}/m^2. X-ray diffraction line profile analysis was performed to characterize the microstructural parameters of these samples. Average domain size, microstrain and dislocation density were estimated as a function of dose. An anomaly was observed in the values of these parameters at a dose of 2×10^{18} O^{5+}/m^2. Positron annihilation spectroscopy was used to determine the existence and nature of vacancy clusters in the samples. Isochronal annealing was carried out for a sample to study the evolution of defect clusters.**

Keywords. **Microstructure; defects; X-ray diffraction technique; positron annihilation spectroscopy.**

1. Introduction

Zirconium based alloys are used extensively as the nuclear structural materials in the pressurized heavy water reactors. These alloys have a combination of good corrosion resistance, mechanical properties at elevated temperatures and resistance to irradiation induced dimensional changes (Sabol *et al* 1989). Still there is a search for new zirconium alloys for meeting the demands of high burn up fuels, higher coolant temperature and partial boiling of coolant. In this respect, binary Zr–Nb alloys containing about 0·5–2% Nb and quaternary Zr–Nb–Sn–Fe alloys have shown considerable promise (Sabol *et al* 1989, 1991; Nikulina *et al* 1996).

The mechanical properties of zirconium based alloys at high temperature are mainly affected by alloying elements, precipitates and microchemistry. Several advanced zirconium based alloys, such as Zirlo (Zr–1Nb–1Sn–0·1Fe), Zr–1Nb, Zr–0·1Nb–1·0Sn–0·2Fe–0·1Cr have been developed as candidate materials for fuel cladding tube which can support higher fuel burn up and a higher operating temperature. The irradiation induced point defects play a significant role on the microstructure, mechanical and creep properties of these alloys (Nikulina *et al* 1996). Several irradiation studies have been performed on zirconium based alloys over the past forty years. It is found that the nature of production of defects is very complex and depends on initial microstructure, alloying elements, type of ions, dose and dose rate. Particularly at low dose and dose rate, a transient regime is observed before attaining a steady state regime where the microstructure is dose dependent. In our earlier study (Mukherjee *et al* 1999) of the microstructure of proton irradiated Zr–1Nb–1Sn–0·1Fe at different doses, we have observed that Nb and Sn played a significant role in suppressing the vacancy agglomeration by forming the solute atom vacancy complexes.

In order to understand the mechanism of evolution of defects in the transient regime, Zr–1Nb samples were irradiated at room temperature with 116 MeV O^{5+} at low doses and at low dose rate. The microstructural parameters of the irradiated samples have been characterized by X-ray diffraction line profile analysis (XRDLPA) and positron annihilation spectroscopy (PAS). During the XRD experiment, X-ray probes an average volume of 10^9 μm^3. Thus the global microstructural information on the irradiated samples could be extracted in a statistical manner using XRDLPA. On the contrary, PAS provides the intrinsic characteristics of the lattice defects in a much shorter length scale. Hence, information obtained from these two techniques are complementary and possibly gives a detailed account of the irradiated microstructure in a non-destructive way.

2. Experimental

Zr–1Nb alloy was prepared by hot extrusion and beta-quenching followed by a second hot extrusion and cold rolling. These deformed samples were then annealed at 580°C for 1 h. The thickness of the sample was 0·6 mm.

Samples of dimension 10×10 mm were cut and then irradiated with 116 MeV O^{5+} from variable energy cyclotron (VEC), Kolkata. The irradiation doses were 5×10^{17},

*Author for correspondence (paramita@veccal.ernet.in)

1×10^{18}, 2×10^{18} and 8×10^{18} O^{5+}/m^2. The beam current was kept constant at 150 nA. The flange used in the irradiation was cooled by continuous flow of water. During irradiation, the average temperature of the sample did not rise above 313 K as measured by the thermocouple connected to the closest proximity of the sample. The rise of temperature up to 313 K was attained within 160 s in each case and then became stable at that temperature.

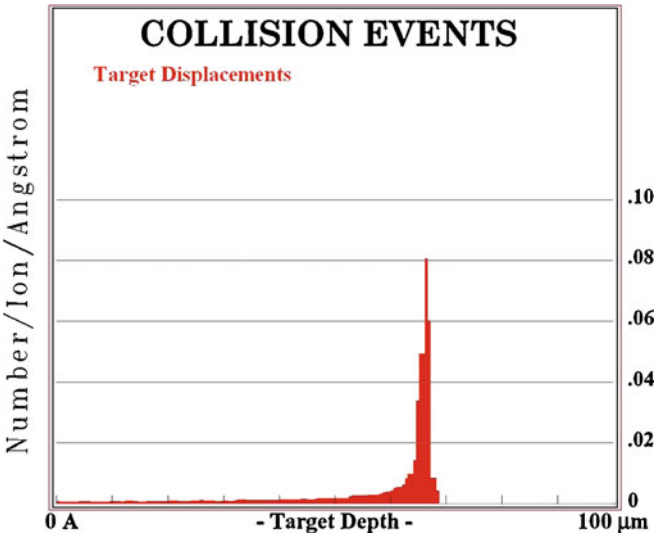

Figure 1. Target displacements by 116 MeV O^{5+} ions on Zr–1Nb alloy.

X-ray diffraction profiles for each irradiated sample have been recorded with the help of Bruker D-8 Advance diffractometer using Cu-Kα radiation. The range of 2θ was 30°–101° with a step scan of 0·02°. The time per step was 20 s.

PAS was performed on the unirradiated and irradiated samples. The positron source used was ^{22}Na with a strength ~10 µCi. The source was covered with a very thin nickel foil (~2 µm thickness) and was sandwiched between two samples having same irradiation doses, such that the irradiated surfaces of the samples face each other. This source-sample assembly was then placed between two BaF_2 detectors. The time resolution of the prompt gamma–gamma coincidence of the circuit was 200 ps as measured by a ^{60}Co gamma source. PAS measurements were also carried out on the specimen irradiated at a dose of 1×10^{18} O^{5+}/m^2 after different stages of isochronal annealing in a temperature range 373–1073 K at an interval of 100 K.

3. Method of analysis

Apart from the instrumental broadening, the broadenings associated with different Bragg peaks in the X-ray diffraction pattern arise due to the microstructural imperfections inside the polycrystalline sample, like domain size and microstrain. This microstructural information can be extracted successfully by analysing the X-ray diffraction pattern using different model based approaches. The Williamson–Hall technique and the modified Rietveld method have been adopted to

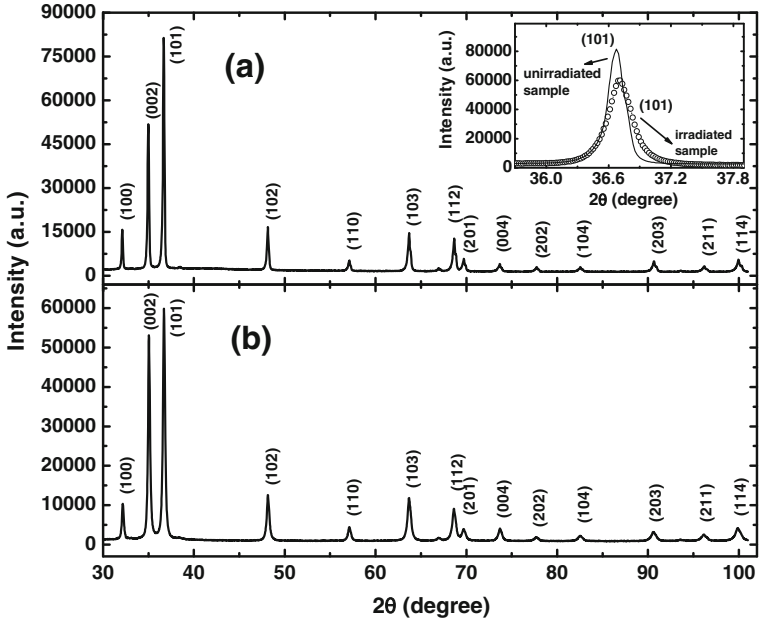

Figure 2. XRD profiles for **(a)** unirradiated sample and **(b)** sample irradiated with 8×10^{18} O^{5+}/m^2. The broadening of the (101) peak for the irradiated sample with respect to the unirradiated one has been shown clearly in the inset.

study the microstructural variation as a function of dose from XRDLPA. The data obtained from PAS have been analysed using the conventional two-state trapping model.

3.1 *Williamson–Hall technique*

According to the Williamson–Hall technique (Williamson and Hall 1953), it is assumed that, both the size and strain broadened profiles are Lorentzian. Based on this assumption, a mathematical relation was established (Williamson and Hall 1953) between the integral breadth (β), the volume weighted average domain size (D_v) and the upper limit of the microstrain (ε) as follows:

$$\frac{\beta\cos\theta}{\lambda} = \frac{1}{D_v} + 2\varepsilon S, \tag{1}$$

where $S = (2\sin\theta/\lambda)$.

The plot of $(\beta\cos\theta/\lambda)$ versus S gives the value of ε from the slope and D_v from the ordinate intercept.

3.2 *Modified Rietveld method*

In this method, the diffraction profiles have been modeled by the pseudo-Voigt function using the program LS1 (Lutterotti and Scardi 1990). This program simultaneously refines the crystal structures, microstructural parameters like surface weighted average domain size (D_S), average microstrain $\langle\varepsilon_L^2\rangle^{1/2}$ and the preferred orientation parameter, assuming the isotropicity in the domain size and microstrain. Preferred orientation correction parameter $P(\alpha)$ (Dollase 1986; Will *et al* 1988) has the form

$$P(\alpha) = \left(r^2\cos^2\alpha + \frac{\sin^2\alpha}{r}\right)^{-\frac{3}{2}}, \tag{2}$$

where α is the angle between *hkl* and the preferred oriented plane and r is an adjustable parameter. XRD peak profile of Zr–1Sn–1Nb–0·1Fe shows strong crystallographic texture along certain crystallographic directions, particularly (002) and (101). The h, k, l values of these planes were incorporated in the programme as preferred oriented planes and the best fit was sought in each case. Having obtained the values of average D_S and $\langle\varepsilon_L^2\rangle^{1/2}$ from isotropic model, the average domain size and strain were further refined to calculate effective domain size and microstrain for each crystallographic plane. Considering the X-ray line profiles to be symmetric in shape, the distributions of dislocations were assumed to be random. The average dislocation density (ρ) has been estimated from the relation (Williamson and Smallman 1956)

$$\rho = (\rho_D\rho_S)^{\frac{1}{2}},$$

where $\rho_D = 3/D_S^2$ (density of dislocation due to domain) and $\rho_S = k\langle\varepsilon_L^2\rangle/b^2$ (density of dislocation due to strain), k is the material constant and b the modulus of the Burger's vector $\frac{1}{3}[11\bar{2}0]$.

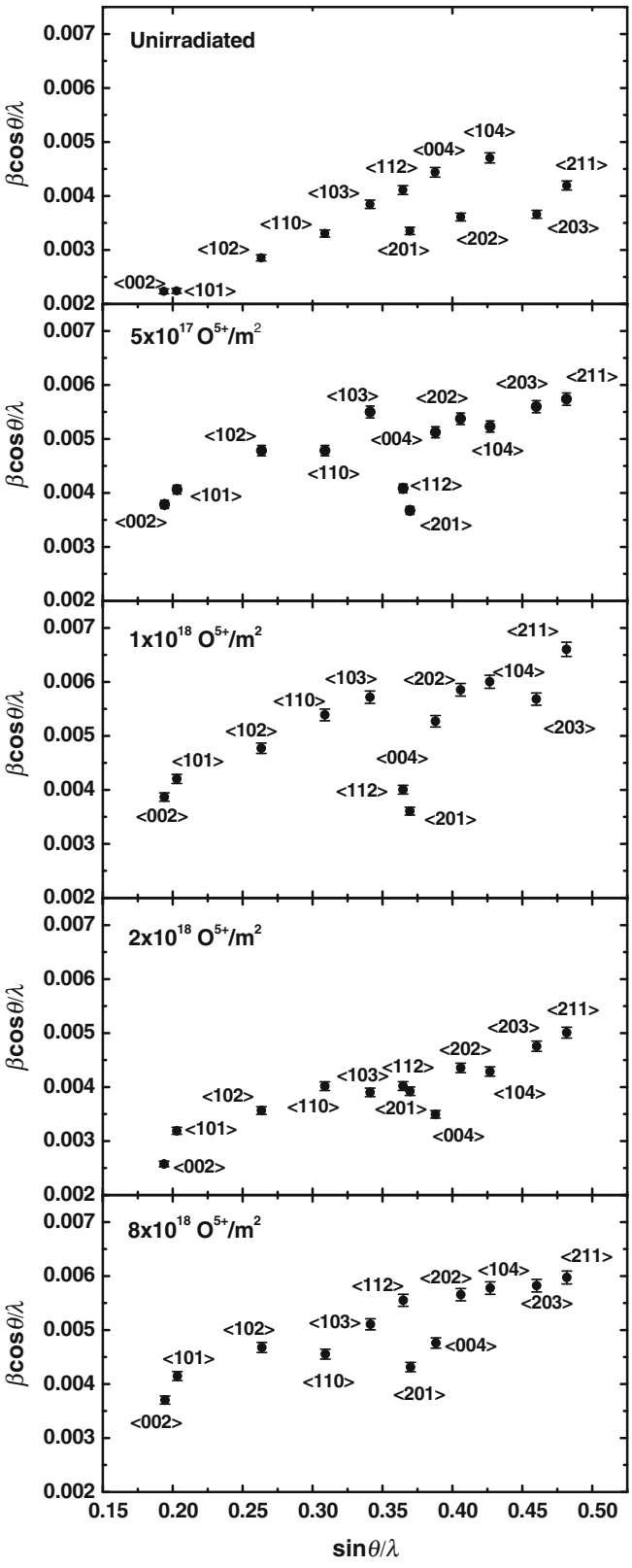

Figure 3. Williamson–Hall plot of Zr–1Nb samples at different irradiation doses.

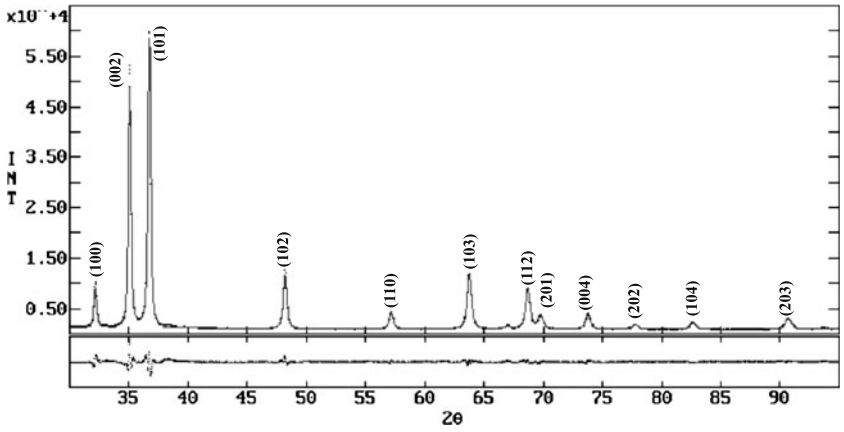

Figure 4. Rietveld fit for the diffraction profile of the oxygen-irradiated Zr–1Nb sample at a dose of 8×10^{18} O^{5+}/m^2. Residuals of the fit are also shown in the lower box.

3.3 *Analysis of PAS data*

The data obtained from PAS has been analysed using the conventional two-state trapping model (Hautojarvi and Corbel 1995). It is assumed in this model that the positrons can either annihilate in the free state in the bulk with a rate λ_b or annihilate after being trapped into a vacancy type defect with a reduced rate λ_t. At a given instant of time t, if n_b and n_t are the number of positrons in the bulk and the defects respectively, the two rate equations governing the annihilation processes can be written as (Hautojarvi and Corbel 1995)

$$\frac{dn_b}{dt} = -n_b\lambda_b - n_b\kappa_t, \tag{3}$$

and

$$\frac{dn_t}{dt} = -n_t\lambda_t + n_b\kappa_t, \tag{4}$$

where κ_t is the rate of trapping of positrons by the defects. Assuming that the positrons are initially released into the bulk and the number of trapped positrons $n_t = 0$ at $t = 0$, these equations can be solved to represent the measured positron lifetime spectrum as

$$N(t) = I_1 \exp(-t/\tau_1) + I_2 \exp(-t/\tau_2), \tag{5}$$

where $\tau_1 = (\lambda_b + \kappa_t)^{-1}$ and $\tau_2 = \lambda_t^{-1}$ are the two measured positron lifetimes and $I_1 + I_2 = 100\%$.

4. Results

The range of 116 MeV O^{5+} in Zr–1Nb is estimated to be around 66 μm by SRIM 2003 (Biersack and Haggman 1980). The radiation damage was assayed by the damage energy deposited causing displacement of atoms. Figure 1 shows the total target displacement of the collision events in Zr–1Nb alloy estimated using SRIM 2003. The maximum dpa at the peak region for the sample at a dose of 8×10^{18} O^{5+}/m^2 was found to be 0·15.

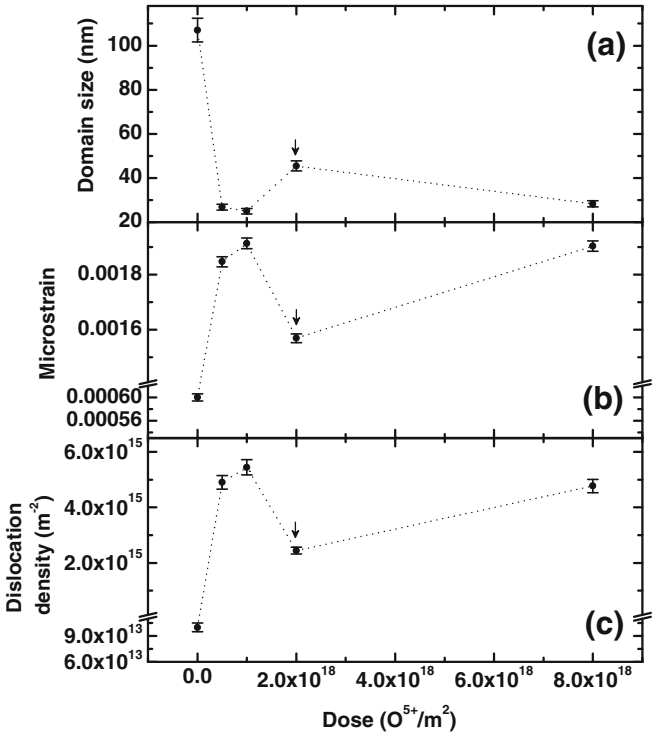

Figure 5. Variation of **(a)** average domain size, **(b)** average microstrain and **(c)** average dislocation density with different irradiation doses.

4.1 *X-ray diffraction line profile analysis (XRDLPA)*

Figure 2 represents the typical X-ray diffraction profiles of the unirradiated sample and the sample irradiated to a dose of 8×10^{18} O^{5+}/m^2. The broadening seen clearly in the XRD profile (inset of figure 2) of the irradiated sample has resulted

Table 1. Effective domain size, microstrain and dislocation density along different crystallographic planes for the Zr–1Nb sample irradiated to different doses (O^{5+}/m^2).

Dose (O^{5+}/m^2)	Domain size (nm) Error = ±2				Microstrain (10^{-3}) Error = ± 10^{-5}				Dislocation density (10^{15}) (m^{-2}) Error = ±(5.4×10^{13})			
	Unirradiated	5×10^{17}	1×10^{18}	2×10^{18}	8×10^{18}	Unirradiated	5×10^{17}	1×10^{18}	2×10^{18}	8×10^{18}	Unirradiated	5×10^{17}	1×10^{18}	2×10^{18}	8×10^{18}
002	107	30	30	51	34	0·6	1·91	1·94	1·52	1·94	0·1	4·52	4·60	2·10	4·05
101	106	30	26	46	34	0·6	1·86	1·95	1·55	1·70	0·2	4·37	5·24	2·39	3·52
102	109	30	29	49	34	0·7	1·89	1·94	1·53	1·85	0·1	4·46	4·83	2·20	3·84
103	111	30	29	50	34	0·7	1·90	1·94	1·53	1·89	0·2	4·49	4·71	2·15	3·95
112	107	29	26	47	32	0·7	1·88	1·92	1·54	1·89	0·2	4·66	5·16	2·32	4·24

due to the microstructural changes (particularly in the domain size and microstrain) caused by heavy ion irradiation.

Figure 3 shows the W–H plot for the unirradiated and the irradiated Zr–1Nb samples at different doses. The points corresponding to each crystallographic plane are found to be scattered in the plots for the unirradiated sample and also for the sample irradiated at a dose of 5×10^{17} O^{5+}/m^2. This scattered nature of the points in the plots implies a strong anisotropy in the domain size and microstrain along different crystallographic directions. But with increasing dose of irradiation, the points in the plots are found to be less scattered and almost shows a linear trend at the dose of 2×10^{18} O^{5+}/m^2. However, the relative intensities of the XRD peaks did not change much due to irradiation at different doses, which indicate that the initial texture has not changed due to irradiation. Hence, the scattered nature of the W–H plots is mainly due to changes in the microstructural parameters like domain size and microstrain caused by irradiation.

Figure 4 shows a typical Rietveld fit for the Zr–1Nb sample with highest dose of irradiation (8×10^{18} O^{5+}/m^2). The variations of D_s, $\langle\varepsilon_L^2\rangle^{1/2}$ and ρ as a function of irradiation dose obtained from the modified Rietveld method have been shown in figure 5. A sharp decrease in the domain size (figure 5a) and increase in the microstrain (figure 5b) are observed at the initial stages of irradiation which tends to saturate at higher irradiation doses except at a dose of 2×10^{18} O^{5+}/m^2 (marked by arrow). Figure 5(c) reveals the variation of dislocation density as a function of irradiation dose. The density of dislocation increases with dose but shows an anomaly at that particular dose of 2×10^{18} O^{5+}/m^2. The values of the effective domain size D_e, microstrain and dislocation density along different crystallographic planes are shown in table 1. These data in table 1 also show the anomaly at the same dose of irradiation.

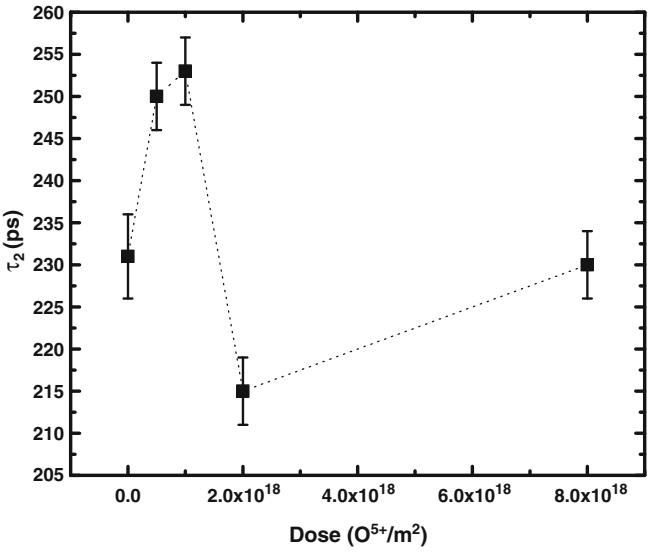

Figure 6. Variation of τ_2 with irradiation doses.

Table 2. Values of τ_1, τ_2 and I_2 for the unirradiated and irradiated samples.

Irradiation doses (O^{5+}/m^2)	τ_1 (ps)	τ_2 (ps)	I_2
Unirradiated	128 ± 3	231 ± 5	$43{\cdot}4 \pm 3{\cdot}4$
5×10^{17}	132 ± 2	250 ± 4	$47{\cdot}7 \pm 2{\cdot}4$
1×10^{18}	137 ± 3	253 ± 4	$50{\cdot}7 \pm 2{\cdot}8$
2×10^{18}	119 ± 4	215 ± 4	$56{\cdot}1 \pm 3{\cdot}8$
8×10^{18}	125 ± 4	230 ± 4	$52{\cdot}3 \pm 3{\cdot}7$

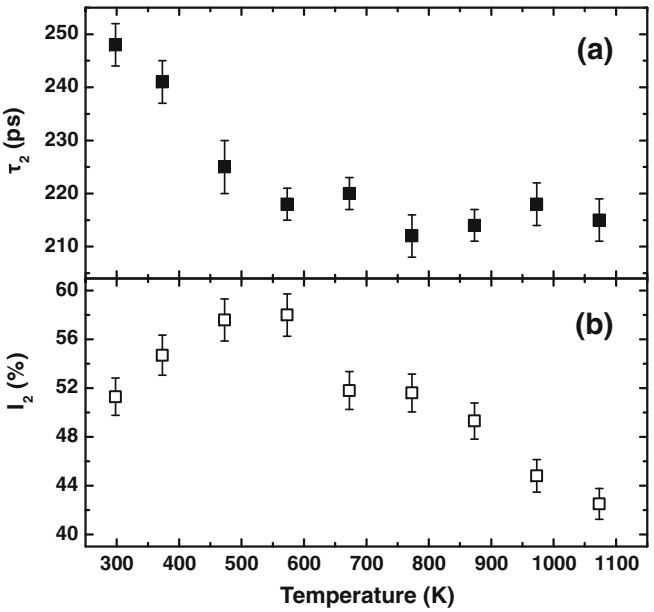

Figure 7. Variation of **(a)** τ_2 and **(b)** I_2 with isochronal annealing temperature.

4.2 *Positron annihilation spectroscopy (PAS)*

The variation of the positron life time τ_2 as a function of irradiation dose is shown in figure 6. In this case also, we observe similar kind of anomaly at the same dose of irradiation (2×10^{18} O^{5+}/m^2). The values of τ_1, τ_2 and I_2 found from the PAS study are listed in table 2.

Isochronal annealing studies by PAS have been performed on the sample with a dose of 1×10^{18} O^{5+}/m^2. Figure 7(a) shows the variation of τ_2 with respect to the annealing temperature. We observed a drastic fall of τ_2 up to a temperature of 573 K, followed by saturation to 215 ps at higher annealing temperatures. The variation of I_2 with temperature is shown in figure 7(b), which exhibits a peak at 573 K.

5. Discussion

The radiation damage by heavy ions (O^{5+}) is essentially characterized by the displacement cascade consisting of highly localized interstitials and vacancies. These mobile point defects interact with the microstructure by long range diffusion (Abromeit *et al* 1994). The main mechanism of the migration of point defects and their annihilation are based on three reaction paths (i) the loss of point defects at extended sinks such as surfaces, grain boundaries, and at the network of the existing dislocations, (ii) the nucleation of the clusters by the homogeneous reaction between the point defects of the same type and (iii) the growth of the defect clusters like the dislocation loops and voids by agglomeration of the point defects.

In the irradiated sample, the enhancement of radiation induced diffusion is solely responsible for the migration of vacancies, their agglomeration and collapsing in the shape of dislocation loops. The generation of dislocation by collapsing of vacancy clusters is only possible when there is vacancy concentration in excess of the equilibrium values. We could observe an order of magnitude increase in the density of dislocation at the initial stages of irradiation, which in turn can act as a sink for vacancies. Hence, the annihilation of vacancies also takes place during irradiation as a competing process to the generation of vacancies. With the increase in dose of irradiation, the annihilation of vacancies increases because of the formation of new dislocation loops due to the collapse of vacancy clusters. When the rate of annihilation of vacancies is comparable to the rate of its generation, a saturation of the dislocation density occurs. This effect has also been observed in our earlier studies on Zr–1Sn–1Nb–0·1Fe (Sarkar *et al* 2008; Mukherjee *et al* 2002, 2005) irradiated with $Ne^{6+}$and O^{5+} ions. But in case of proton (light ion) irradiation studies (Mukherjee *et al* 2001), we did not observe any clustering beyond trivacancy clusters even up to the highest dose of irradiation characterized by PAS. We also did not observe any significant change in the dislocation density in the proton irradiated Zr–1Nb–1Sn–0·1Fe samples (Mukherjee *et al* 2001).

In our present work, we have observed a sudden decrease in the dislocation density at a specific irradiation dose of 2×10^{18} O^{5+}/m^2 (figure 5c). To explain this anomaly we take recourse to the PAS results obtained in our samples. From figure 6, the value of the positron life time in the unirradiated sample (231 ps) corresponds to that of a monovacancy in pure Zr (228 ps) as reported in the literature (Campillo Robles *et al* 2007). The value of τ_2 in the irradiated samples indicates the presence of mono and di-vacancies except again at a dose of 2×10^{18} O^{5+}/m^2 where the value is 215 ps. This low value of τ_2 indicates that there are no dominant vacancies at this dose and thus can be attributed to the presence of dislocation loops alone (Hatakeyama *et al* 2009). The absence of vacancies and the lower value of dislocation density at this dose (figure 5c) can be explained as follows. At the particular dose of irradiation, if the rate of annihilation of vacancies into the sink (dislocation loops) dominates over the rate of their creation, a situation may arise where all the vacancies that are created gets annihilated in the sinks thus lowering the sink density (dislocation density) itself. In our earlier studies of irradiation on Zr–1Sn–1Nb–0·1Fe (Mukherjee *et al* 2002;

Sarkar *et al* 2008) by Ne^{6+} and O^{5+} energetic ions we did not observe this anomaly.

In case of the isochronal annealing studies on the 1×10^{18} O^{5+}/m^2 sample, the drastic fall of τ_2 (figure 7a) up to a temperature of 573 K has been observed due to the annihilation of the vacancies. As observed in figure 7(b), the initial increase in I_2 can be attributed to the increase in the concentration of mono-vacancies resulting from the dissociation of vacancy-impurity complexes. Upadhyaya and Muraleedharan (1987) observed the dissociation of vacancy–impurity complexes in Zr–0·5Nb system around a temperature of 523 K. According to Cottrell (1967), the following relation approximately describes the binding energy of a vacancy with a foreign atom which has a size misfit, "η", with the matrix lattice:

$$E_b = 8\pi\mu r_0^3 \eta^2, \tag{6}$$

where μ is the shear modulus of the matrix, r_0 the matrix atom radius and

$$\eta = \pm\left(\frac{r_1 - r_0}{r_0}\right), \tag{7}$$

where r_1 is the impurity atom radius. Using (6), E_b for vacancy–niobium complexes in zirconium matrix is found to be around 0·08 eV which corresponds to a temperature around 619 K. This value approximately matches with the peak temperature observed in figure 7(b).

6. Conclusions

The microstructural parameters like average domain size, microstrain and dislocation density of the 116 MeV O^{5+} irradiated Zr–1Nb alloy have been obtained reliably using XRDLPA in the low dose regime. An anomaly was observed in the value of these parameters at a specific dose of 2×10^{18} O^{5+}/m^2 which indicates that the irradiation induced microstructure in this alloy is very much dose dependent in this low dose regime. PAS results also reveal the same anomaly at this specific dose corroborating the above results. Isochronal annealing studies using PAS gives the signature of the presence of vacancy–solute atom complexes at the initial stages of annealing, which gets dissociated at higher annealing temperatures.

References

Abromeit C 1994 *J. Nucl. Mater.* **216** 78

Biersack J P and Haggmark L G 1980 *Nucl. Instrum. Methods* **174** 257 (The Stopping and Range of Ions in Matter (SRIM 2000) software developed by Ziegler J and Biersack J P is available on the Website http://www.research.ibm.com/ionbeams)

Campillo Robles J M, Ogando E and Plazaola F 2007 *J. Phys. Condens. Matter* **19** 176222

Cottrell A H 1967 *An introduction to metallurgy* (London: Edward Arnold)

Dollase W A 1986 *J. Appl. Crystallogr.* **19** 267

Hatakeyama M, Toyama T, Yang J, Nagai Y, Hasegawa M, Ohkubo T, Eldrup M and Singh B N 2009 *J. Nucl. Mater.* **386** 852

Hautojarvi P and Corbel C 1995 *Positron spectroscopy of defects in metals and semiconductors*, in *Positron spectroscopy of solids* (eds) A Dupasquier and AP Mills, IOS press, p. 491

Lutterotti L and Scardi P 1990 *J. Appl. Crystallogr.* **23** 246

Mukherjee P, Nambissan P M G, Sen Pintu, Barat P and Bandyopadhyay S K 1999 *J. Nucl. Mater.* **273** 338

Mukherjee P, et al 2001 *J. Nucl. Mater.* **297** 341

Mukherjee P, Barat P, Bandyopadhyay S K, Sen P, Chottopadhyay S K, Chatterjee S K and Mitra M K 2002 *J. Nucl. Mater.* **305** 169

Mukherjee P, Sarkar A and Barat P 2005 *Mater. Char.* **55** 412

Nikulina A V, Markelov V A, Peregud M M, Voevodin V N, Panchenko V L and Kobylyansky G P 1996 *J. Nucl. Mater.* **238** 205

Sabol G, Klip G R, Balfour M G and Roberts E 1989 *Zirconium in nuclear industry*, *Eighth international symposium* (ASTM STP), Philadelphia, **1023** 227

Sabol G P, Schoenberger G and Balfour M G 1991 *IAEA tech. comm. meeting on materials for advanced water-cooled reactors*, *Plzen, Czech and Slovak Federal Republic*, IAEA, p. 50

Sarkar A, Mukherjee P and Barat P 2008 *J. Nucl Mater.* **372** 285

Upadhyaya D D and Muraleedharan R V 1987 *Bull. Mater. Sci.* **9** 235

Will G, Belloto M, Parrish W and Hatr M 1988 *J. Appl. Crystallogr.* **21** 182

Williamson G K and Hall W H 1953 *Acta Metall.* **1** 22

Williamson G K and Smallman R E 1956 *Philos. Mag.* **1** 34